Table S1: Statistics of the M3C2 comparison between the 28/05/2024 15:00 time-lapse point clouds obtained with 3, 4 and 5 cameras relative to the concurrent UAV point cloud.

	5 cameras	4 cameras	3 cameras
Number of points	2,048,278	1,812,222	1,515,636
Absolute mean (m)	1.0	0.5	0.2
Standard deviation (m)	4.4	2.8	3.2
RMSE (m)	4.5	2.9	3.2

Table S2: Statistics of the M3C2 comparison between the 27/09/2023 12:00 time-lapse point clouds obtained with 3, 4 and 5 cameras relative to the time-lapse point cloud from the same date and time obtained with 7 cameras (2,331,388 points).

	5 cameras	4 cameras	3 cameras
Number of points	2,359,898	2,293,079	1,938,892
Absolute mean (m)	0.5	0.3	0.3
Standard deviation (m)	3.6	3.1	1.9
RMSE (m)	3.6	3.1	2.0

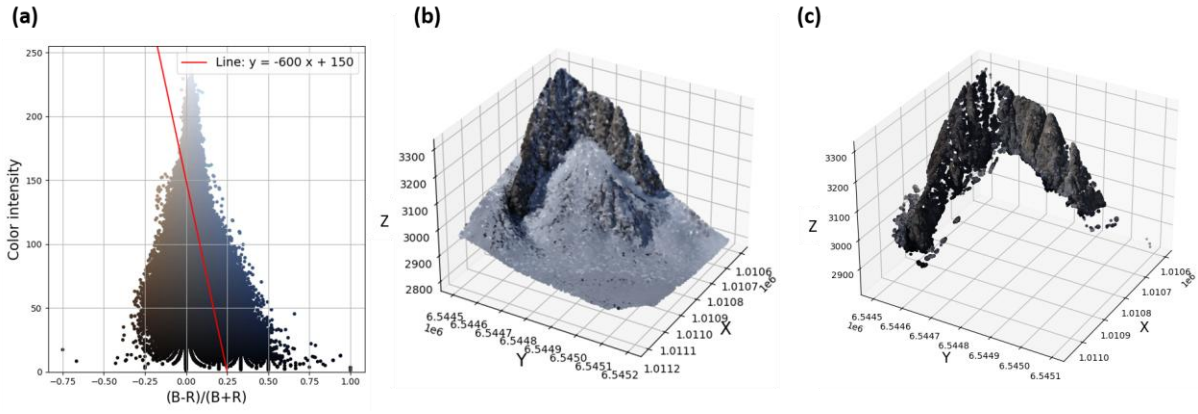

Figure S1: Extraction of stable terrain based on point colour. (a) extraction of all the points below the red line as stable rock. The colour intensity corresponds to the mean value of the red (R), green (G) and blue (B) bands. (b) 27/09/2023 point cloud before extraction of the stable terrain. (c) 27/09/2023 point cloud after extraction of the stable terrain. For readability the point clouds in the figure were downsampled by a factor 100.

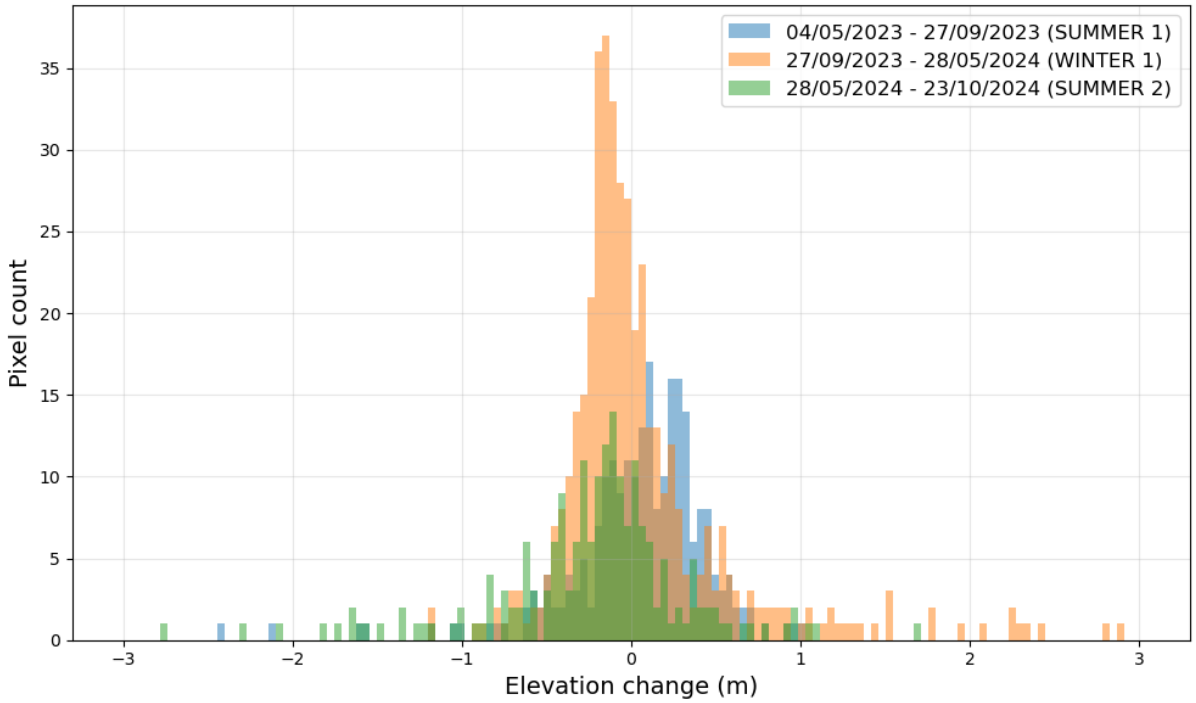

Figure S2: Histograms of elevation change over manually defined stable terrain for the different elevation change maps. 3% of the points fall out of the range and are considered to be outliers.

Figure S3: Time-lapse camera setup and installation. (a) time-lapse camera mounted onto a rock outcrop. (b) Installation of Camera 2 at the start of the fieldwork. (c) Revisit of Camera 2 location two months later. The red triangle indicates the location of the camera (identical position in both images).

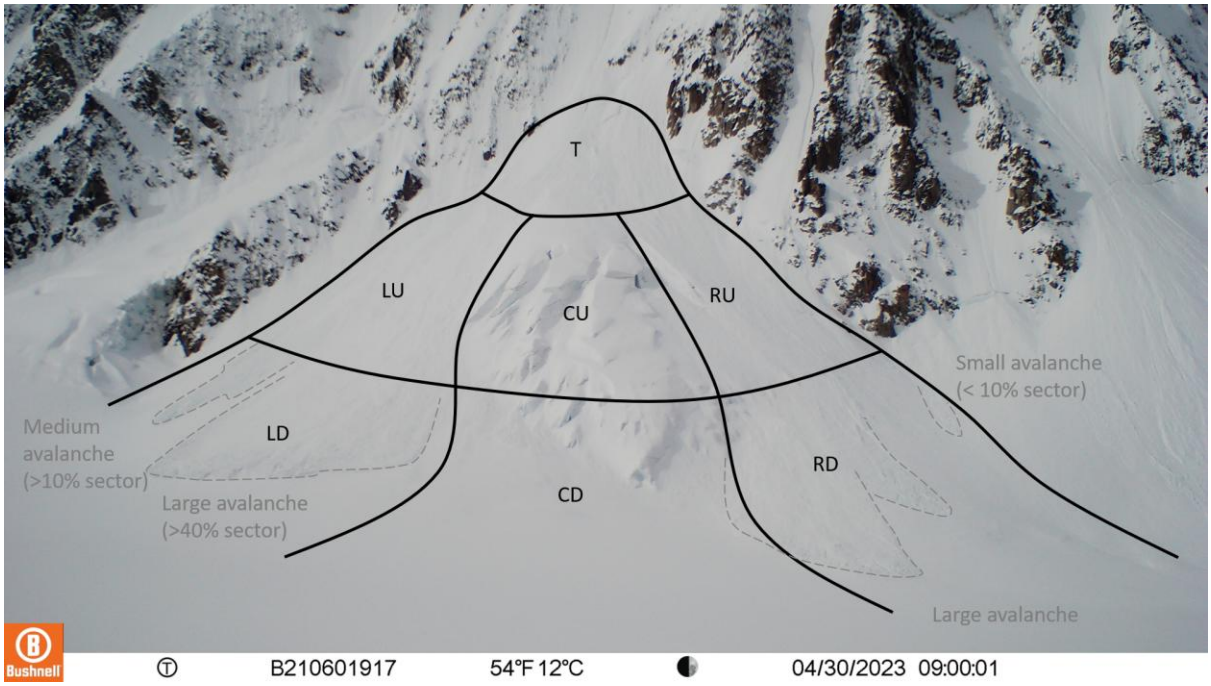

Figure S4: Different sectors of the avalanche cone used to categorize avalanche deposits based on their size and extents. T: Top of cone. LU: Left-Up. CU: Center Up. RU: Right Up. LD: Left Down. CD: Center Down. RD: Right Down.

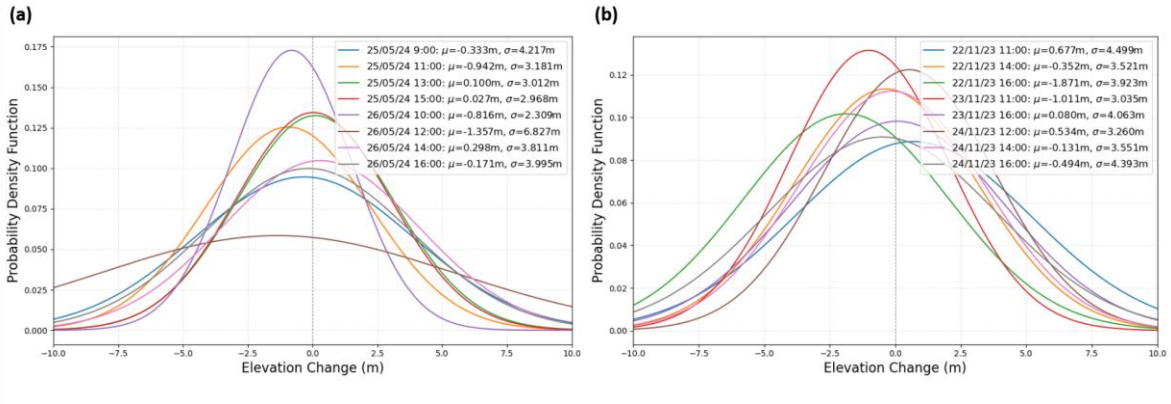

Figure S5: Probability density function (PDF) of the elevation change between time-lapse DEMs acquired within 48-hours of one another, relative to a reference DEM from the same period. These elevation changes therefore represent the error, since we do not expect any changes during such short time periods. (a) Elevation change PDFs of time-lapse DEMs acquired between 25/05/2024 09:00 and 26/05/2024 16:00, relative to the reference time-lapse DEM from 26/05/2024 08:00. (b) Elevation change PDFs of time-lapse DEMs acquired between 22/11/2023 11:00 and 24/11/2023 16:00, relative to the reference time-lapse DEM from 23/11/2023 14:00. μ corresponds to the mean and σ to the standard deviation of the elevation change distribution. The PDFs were shown instead of the histograms to improve visibility.

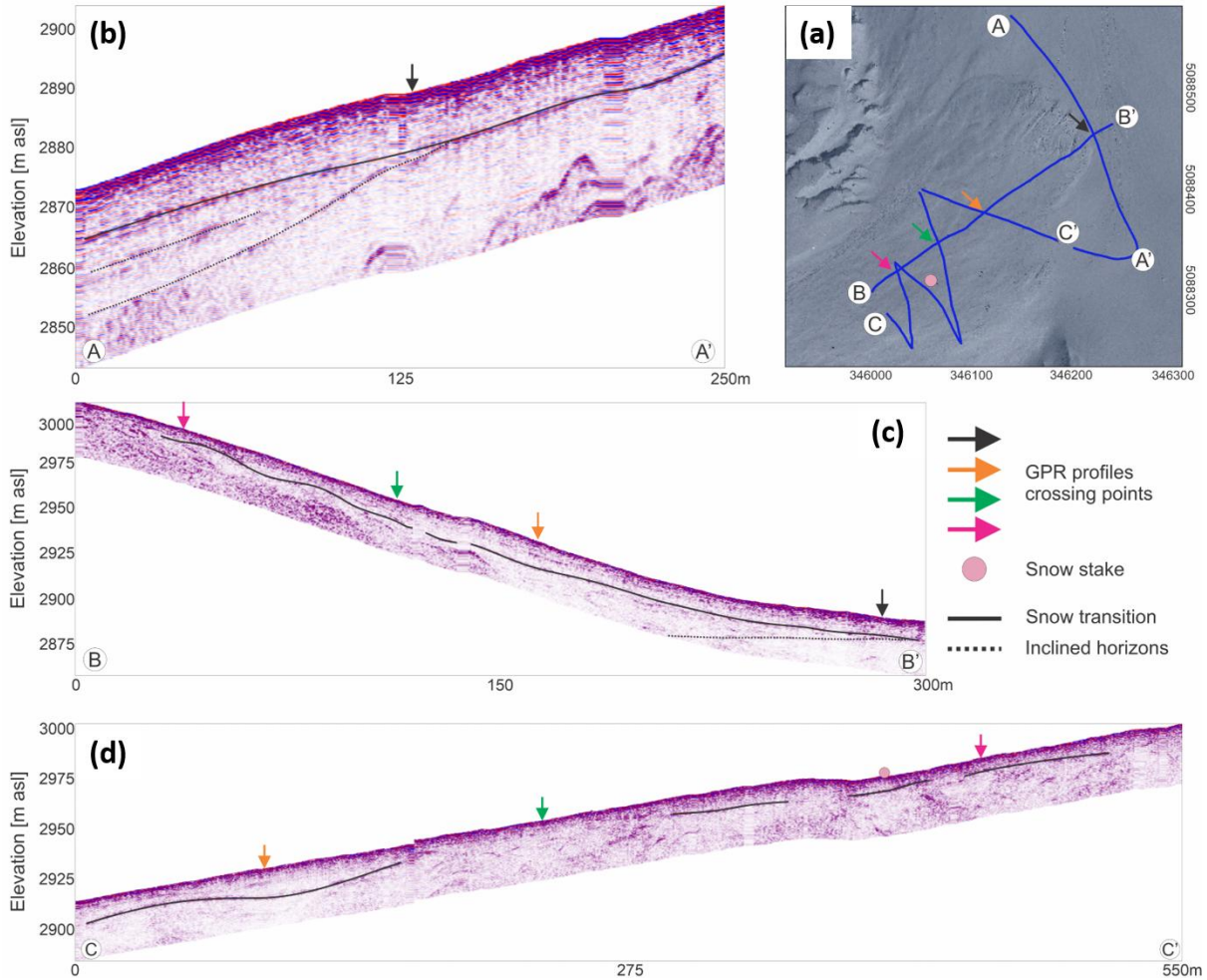

Figure S6: GPR profiles conducted with a 250 MHz antenna on the lower part of the cone on 4 May 2023. (a) GPR track on the lower part of the cone. The pink circle corresponds to the location of density profile F3, where the horizon was measured at 6.45 m below the surface. Background image is the 4 May 2023 UAV orthoimage. (b-d) Radargrams of the different acquisition segments with the crossing points indicated by the arrows and the main reflectors identified by the black lines.

Figure S7: Picture of the cone from 11 June 2023, 09:00 CET taken by Camera 5. The black arrows indicate deeply incised runnels, at the base of which avalanche deposits are visible.

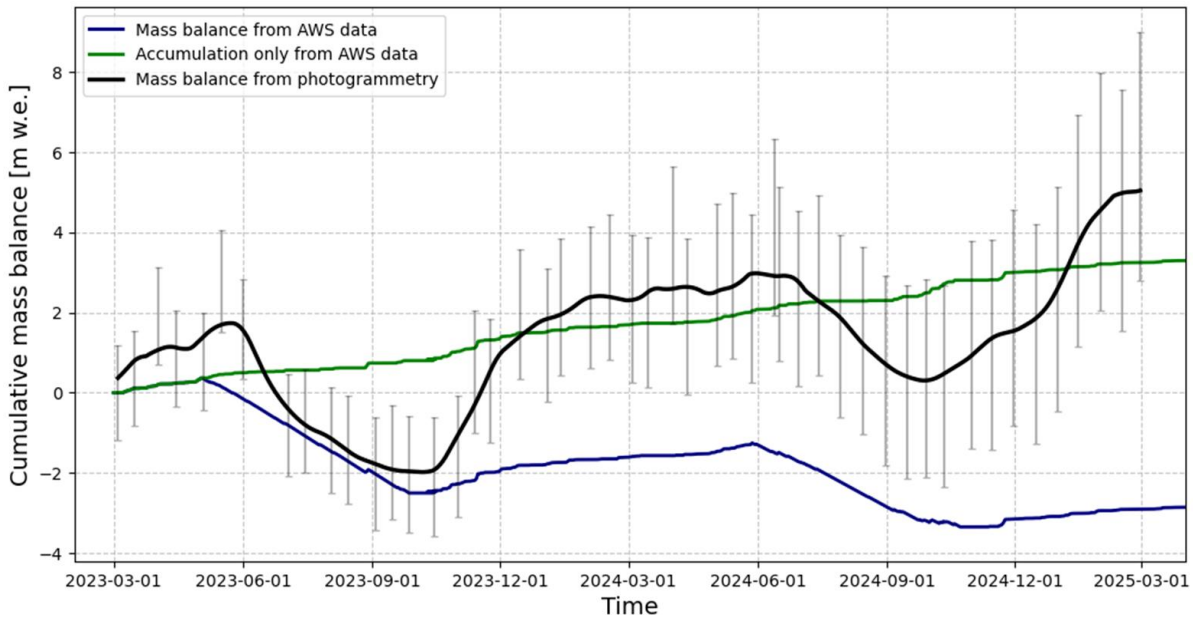

Figure S8: Mass balance of the entire cone based on the solid precipitation on the cone and its headwall only (green), the solid precipitation combined with the measured ablation rates (blue), and the results from the time-lapse photogrammetry.

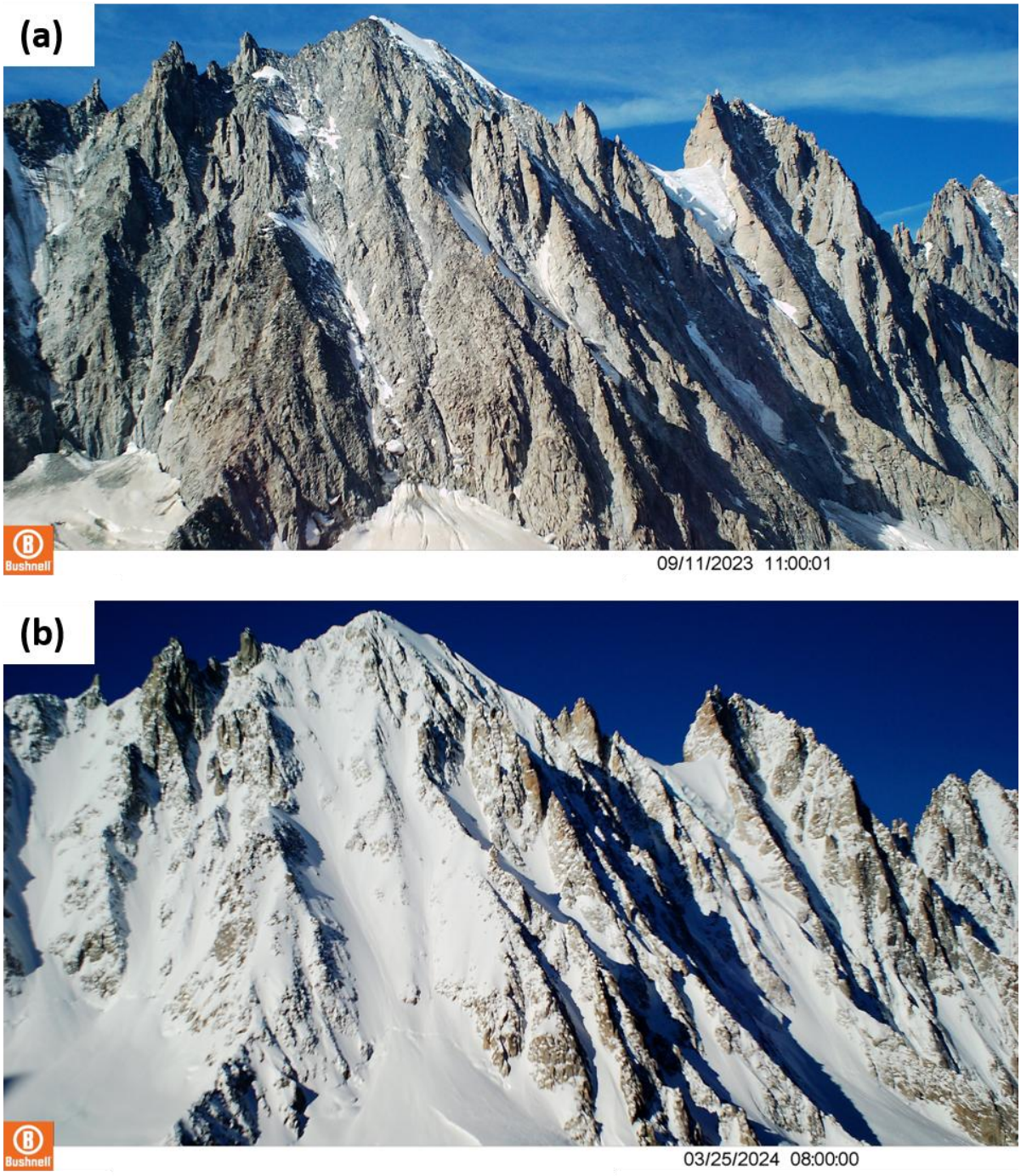

Figure S9: State of the headwall above the cone at different times of the year. (a) Picture from 11 September 2023, at the end of the ablation period. (b) Picture from 25 March, 2024. Both images were captured from the location of Camera 4B.